Paper No.
3744

CORROSION 2014
Collaborate. Educate. Innovate. Mitigate.
March 9-13, 2014 • Henry B. Gonzalez Convention Center • San Antonio, Texas, U.S.A.

Modeling Localized Corrosion of Corrosion-Resistant Alloys in Oil and Gas Production Environments

A. Anderko
OLI Systems Inc.
240 Cedar Knolls Road, Suite 301
Cedar Knolls, NJ 07927
USA

F. Gui, L. Cao, and N. Sridhar
DNV Research and Innovation
5777 Frantz Road
Dublin, OH 43017
USA

ABSTRACT

A methodology has been developed for predicting localized corrosion of corrosion-resistant alloys in environments that contain chlorides and H_2S at conditions that are relevant to oil and gas production. The key element of this methodology is the computation of the repassivation potential, which defines the threshold condition for the existence of stable pits or crevice corrosion. An alloy is susceptible to localized corrosion if the corrosion potential exceeds the repassivation potential. Furthermore, experimental evidence indicates that the repassivation potential also provides a threshold condition for stress corrosion cracking. To understand and predict the effects of environmental conditions and alloy composition on localized corrosion, a mechanistic model has been developed to calculate the repassivation potential in environments containing Cl^- ions and H_2S. The effect of H_2S is complex as its presence may give rise to a strong enhancement of anodic dissolution in the occluded environment and/or the formation of solid metal sulfide phases, which compete with the formation of the oxide in the process of repassivation. The model elucidates the conditions at which H_2S increases the propensity for localized corrosion and those at which it does not. It has been verified using extensive repassivation potential data for a 13-Cr supermartensitic stainless steel (S41425) and more limited data for a 25Cr duplex stainless steel (S32750).

Key words: Localized corrosion, stress corrosion cracking, corrosion-resistant alloys, hydrogen sulfide corrosion, repassivation potential

INTRODUCTION

Corrosion behavior of corrosion-resistant alloys (CRAs) in oil and gas production environments has been attracting significant attention over the past two decades due to a marked trend towards increasing severity of corrosive environments in terms of temperature, pressure, and aggressive species. This trend, coupled with increasing scrutiny of production systems by regulators and the public, is expected to continue in the future and provides impetus to a reexamination of materials selection approaches.

At present, materials specification is based on a combination of standard tests (e.g., NACE TM-01-77[1]), fit-for-purpose testing, and experience. The empirical knowledge is embodied in standards, such as ISO 15156,[2] guidance documents and company specifications. The boundaries of acceptable performance of CRAs are often specified in terms of empirically determined ranges of H_2S and CO_2 partial pressures. However, such approaches may not be satisfactory because the performance of CRAs depends on many other factors such as temperature, acidity, chloride concentration, elemental sulfur, etc., which in turn may depend on complex chemical and phase equilibria in downhole environments. Furthermore, the relationship between accelerated laboratory tests and the actual field environment is often not quantified. Essentially, the performance of a given material needs to be understood in terms of its reliability in a given set of environmental conditions. Therefore, it is of interest to develop a predictive approach that covers a broad range of alloy-environment combinations using a limited set of experimental data coupled with a physical model that is capable of generalizing the experimental database and extrapolating from laboratory tests to field conditions.

From the point of view of CRAs in severe well environments, stress corrosion cracking is of great interest because it can occur over wide ranges of conditions, including the moderate to high temperatures that are critical to downhole applications. For mapping the environmental ranges of SCC, it is crucial to identify a critical potential above which SCC can occur. SCC can be triggered if the corrosion potential of the metal (E_{corr}) exceeds the critical potential. It is generally recognized that localized corrosion can be a precursor to SCC.[3] This is due to the fact that the conditions that lead to localized corrosion (i.e., those that sustain a critical chemistry in an occluded environment inside a pit or crevice) are similar to the conditions that are needed to sustain SCC. For example, experimental evidence exists that SCC in chloride-thiosulfate solutions occurs at potentials above the repassivation potential (E_{rp}) for localized corrosion, thus indicating that localized corrosion leads to the initiation of SCC.[4] Also, the same authors have shown through fracture mechanics testing that measurable crack growth occurs only at potentials more positive to E_{rp}. This indicates that a reliable methodology for the prediction of SCC should be closely linked to the prediction of localized corrosion. Therefore, a joint industry project has been undertaken to:

(1) Develop a comprehensive model for predicting the repassivation potential using a set of new E_{rp} measurements that capture the effects of key electrochemically active species such as Cl^- and H_2S;
(2) Develop a model for predicting the corrosion potential of CRAs in oil and gas production environments; a combination of the E_{corr} and E_{rp} models will make it possible to predict the occurrence of localized corrosion;
(3) Experimentally verify the hypothesis that the repassivation potential for localized corrosion is the appropriate critical potential above which SCC occurs.

In this work, we focus on part (1). Parts (2) and (3) will be the subject of separate studies.

To develop a model for predicting the repassivation potential in oil and gas environments, we extend a previously developed model[5] for calculating E_{rp} in environments containing chlorides and various inhibitive oxyanions. A particularly useful feature of this model is its generalization in terms of composition of Fe-Ni-Cr-Mo-W-N alloys,[6] which makes it possible to predict E_{rp} as a function of not only the environment chemistry but also the alloy composition. However, in its original form, the model is not applicable to systems containing H_2S or other aggressive sulfur species. Various experimental studies have revealed that H_2S and, in general, adsorbed sulfur, has a strong effect on the mechanism of anodic dissolution of individual metals[7-16] and alloys.[17, 18] This effect has a profound influence on the behavior of alloys in occluded environments associated with localized corrosion. Moreover, alloy dissolution and localized corrosion are strongly affected by the formation of metal sulfides.[19-22] Insights from these studies will be utilized to develop a predictive model for the repassivation potential of CRAs in environments containing Cl^- and H_2S as aggressive species. The model will be then verified using

extensive new measurements for a 13-Cr supermartensitic stainless steel (UNS* S41425) and more limited measurements for a 25Cr duplex stainless steel (S32750).

EXPERIMENTAL

Materials and Specimens

Specimens made out of UNS S41425 supermartensitic stainless steel and UNS S32750 duplex stainless steel tubular samples were used in the experiments. The chemical compositions of the two materials are listed in Table 1. Specimens in the form of cylinder and crevice were both used, with the dimensions shown in Figure 1. The creviced specimens were assembled using ceramic multiple-crevice formers wrapped with polytetrafluoroethylene tape. Bolts, nuts and washers were made out of Ti alloy. 70 in.-lb (7.91 N·m) torque was applied on the assembly to ensure the formation of critical crevice geometry for the corrosion-resistant alloys.

Experiment Conditions

Electrochemical experiments were performed in NaCl solutions at various concentrations ranging from 3 molal to 0.0003 molal. All tests were performed at 85°C and ambient pressure. The experiments were conducted with and without the presence of H_2S. In all tests, the solution and the testing vessel were deaerated with research grade nitrogen to remove oxygen. The solution was then transferred to the testing cell under nitrogen to prevent oxygen ingress during solution transfer.

Electrochemical Experiments and E_{rp} Determination

Once the solution was transferred, open-circuit potential (OCP) of the specimen was monitored overnight while the solution was deaerated with nitrogen and subsequently sparged for two hours with H_2S. Following the OCP monitoring, dynamic potential scanning experiments were performed to obtain cyclic polarization curves. The electrochemical cell consisted of a working electrode, a saturated calomel electrode (SCE) as reference in a water-cooled Luggin probe and a Pt/Nb loop as the counter electrode. The dynamic potential scanning was started from -100 mV vs. OCP to 1 V vs. SCE or when the current density reached 1 mA/cm^2, whichever came first. The scanning rate was 0.167 mV/s.

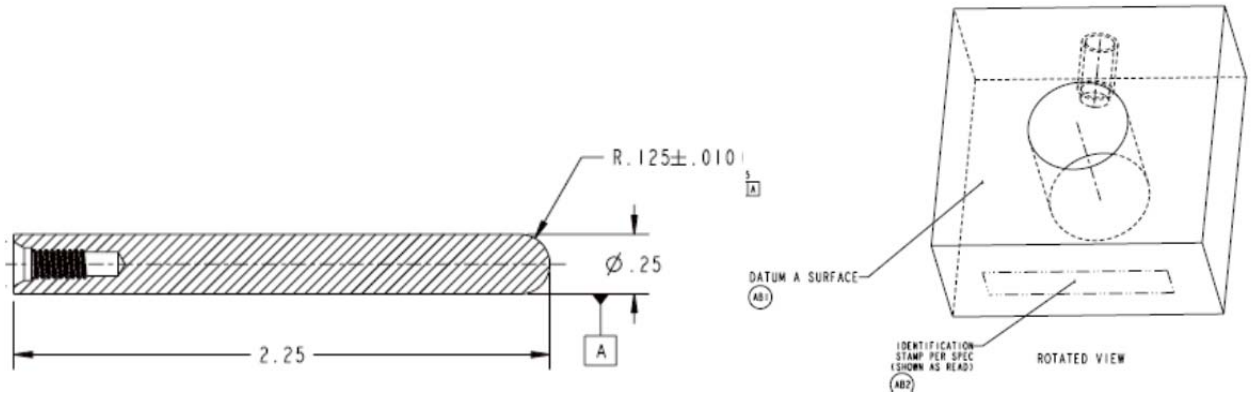

Figure 1. Schematics of the specimens used in the electrochemical experiments for E_{rp} determination

Table 1. Compositions of the alloys studied (weight percent)

Alloy	UNS No	Ni	Fe	Cr	Mo	N	C	Other
S13Cr	S41425	5.90	bal.	12.10	1.90	0	0.010	
2507	S32750	6.93	bal.	25.17	3.87	0.27	0.017	Cu 0.40, Mn 0.8, Si 0.28

* Unified Numbering System for Metals and Alloys (UNS), SAE International and ASTM International

Table 2. Repassivation potentials measured for alloys S41425 and S32750 in Cl^- - H_2S environments at 85°C

Alloy	M (Cl^-) mol/L	wt.% H_2S (gas phase)	Measurement type*	E_{rp} mV (SCE)
S41425	0.0003	0	C	-176
	0.003	0	C	-106
	0.003	0	C	-120
	0.03	0	C	-173
	0.3	0	C	-328
	0.3	0	C	-295
	3	0	B	-400
	3	0	B	-362
	0.0003	1	C	73
	0.003	1	C	8
	0.03	1	C	-200
	0.3	1	C	-146
	0.0003	1	B	362
	0.0003	1	B	396
	0.003	1	B	75
	0.03	1	B	38
	0.03	1	B	-4
	0.3	1	B	-155
	0.3	1	B	-151
	3	1	B	-544
	3	1	B	-554
	0.03	100	C	-368
	0.0003	100	B	-319
	0.0003	100	B	-330
	0.003	100	B	-327
	0.03	100	B	-356
	0.3	100	B	-547
	0.3	100	B	-531
	3	100	B	-593
	3	100	B	-588
S32750	0.003	0	B	995
	0.003	0	B	362
	0.003	0	B	1056
	0.003	0	B	516
	0.03	0	B	568
	0.03	0	B	758
	0.03	0	B	339
	0.3	0	B	19
	0.3	0	B	110
	0.3	0	B	167
	3	0	B	-92
	3	0	B	-102
	3	0	B	-71
	3	0	B	-118
	3	100	B	-519

* C – measurements with crevice samples; B – measurements with boldly exposed surfaces

In typical electrochemical experiments, the repassivation potential (E_{rp}) is selected as the crossover point of the reverse scan portion with the forward scan portion on the polarization curve. In the present work, however, an inflection point appeared often on the reverse scan, indicating the change of passivation. When the anodic current density at the inflection point was within an order of magnitude of the passive current density in the forward scan, the potential at this point was selected to be the E_{rp}. Otherwise, E_{rp} was further confirmed by different electrochemical techniques, i.e. potentiostatic experiments without showing any localized attack for at least 24 hours at a potential ~50mV lower than the inflection point value, and the Tsujikawa-Hisamatsu Electrochemical (THE, also known as potentiodynamic-galvanostatic-potentiostatic) method showing a current transition from increasing to decreasing at potentiostatic holding steps.

The tested specimens were removed from the solution and inspected under an optical microscope or a scanning electron microscope (SEM) to confirm localized corrosion attack. The measured E_{rp} values are collected in Table 2.

COMPUTATIONAL MODEL

Repassivation potential in chloride environments

The repassivation potential model for aqueous systems containing chlorides was described in detail in a previous study.[5] In this section, we describe the fundamentals of this model to create a foundation for a more general model that accounts for the effects of H_2S.

Figure 2 schematically depicts the phases that are considered in an occluded localized corrosion environment. The metal M undergoes an anodic dissolution process below a layer of a non-protective hydrous halide MX with a thickness of *l*. The hydrous halide further dissolves in a solution with a boundary layer thickness *Δ*. In general, the existence of a solid phase MX is not necessary as long as a solution phase with a halide concentration close to saturation is present at the metal interface. The process of repassivation entails the formation of a protective layer of metal oxide MO, which is assumed to cover a certain fraction of the metal surface at a given time. The original E_{rp} model was derived[5] by considering the measurable potential drop across the interface as a sum of four contributions, i.e.,

$$E = \Delta\Phi_{M/MX}(1,2) + \Delta\Phi_{MX}(2,3) + \Delta\Phi_{MX/S}(3,4) + \Delta\Phi_{S}(4,5) \quad (1)$$

where the numbers in parentheses denote the interfaces shown in Fig. 2, $\Delta\Phi_{M/MX}(1,2)$ is the potential difference at the metal/hydrous halide interface, $\Delta\Phi_{MX}(2,3)$ is the potential drop across the hydrous halide layer, $\Delta\Phi_{MX/S}(3,4)$ is the potential difference across the halide/solution interface, and $\Delta\Phi_{S}(4,5)$ is the potential drop across the solution boundary layer. The last three terms in eq. (1) can be evaluated in terms of fluxes and activities of metal and chloride ions using the methods of nonequilibrium thermodynamics introduced by Okada.[23] As described previously,[5] the model is fully determined by the following equations:

(i) An expression for the current density that results from metal dissolution across the (1,2) interface, i.e.,
$$i = i\left(\Delta\Phi_{M/MX}(1,2)\right) \quad (2)$$

(ii) An equation that relates the measurable potential *E* to the current density *i* and the activities of metal ions in the bulk solution ($a_M(5)$) and at the metal interface ($a_M(2)$), i.e.,
$$E = \Delta\Phi_{M/MX}(1,2) + \frac{Ki}{z_M^2 F^2} + \frac{RT}{z_M F}\ln\frac{a_M(5)}{a_M(2)} \quad (3)$$
where *K* is a constant, z_M is the average metal charge and *R* and *F* are the gas and Faraday constants, respectively; and

(iii) A relationship between the activities of chloride ions or other solution species (a_j) and their fluxes in the hydrous halide (J_j') and the boundary layer (J_j''), i.e.,

$$\frac{RT}{z_j F}\ln\frac{a_j(5)}{a_j(2)} = \frac{Ki}{z_M^2 F^2} + \frac{RT}{z_M F}\ln\frac{a_M(5)}{a_M(2)} - \frac{J_j' l}{z_j F \overline{n_j'}\,\overline{v_j'}} - \frac{J_j''\Delta}{z_j F \overline{C_j''}\,\overline{v_j''}} \quad (4)$$

where $\overline{n_j'}$ and $\overline{C_j''}$ are the average concentrations in the hydrous halide and the boundary layer, respectively, and $\overline{v_j'}$ and $\overline{v_j''}$ are the corresponding average mobilities in these phases.

Eqs. (3) and (4) can be simplified in the limit of repassivation when the current density reaches a certain small value, $i = i_{rp}$ (typically, $i_{rp} = 10^{-2}$ A/m^2) and, simultaneously, the fluxes of active species and metal ions become small and comparable to those resulting from passive dissolution. Then, it can be shown that in the limiting case of $E = E_{rp}$, eqs. (3) and (4) simplify to[5]

$$E_{rp} = \Delta\Phi_{M/MX}(1,2) + K_1 \quad (5)$$

$$\frac{a_j(5)}{a_j(2)} \approx K_3 \quad (6)$$

where K_1 and K_2 are constants. To obtain a working equation for E_{rp}, a detailed expression needs to be established for $i\left(\Delta\Phi_{M/MX}(1,2)\right)$ (eq. 2), which reflects the mechanism of active dissolution and oxide formation. Such an expression was proposed in a previous study[5] for environments containing chlorides and inhibitive oxyanions. However, the previously developed expression for $i\left(\Delta\Phi_{M/MX}(1,2)\right)$ is not suitable for H_2S-containing systems because it does not take into account the electrochemical behavior of metal interfaces with an adsorbed sulfur layer.

An expression that satisfies this requirement will be derived in the next section. While a new expression for $i\left(\Delta\Phi_{M/MX}(1,2)\right)$ is necessary for systems in which H_2S(aq) is the dominant corrosive species , eqs. (1-6) still apply. For simplicity, the derivation will be limited to Cl^- and H_2S as electrochemically active species. An extension to multicomponent systems will be presented in a future study.

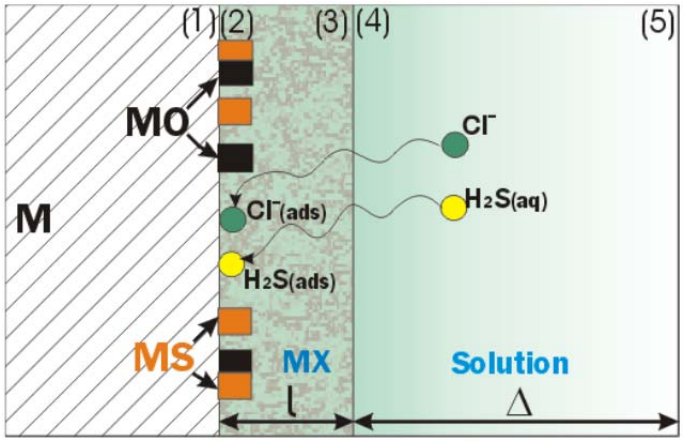

Figure 2. Schematic summary of the phases and interfaces considered in the model (M – metal, MX – hydrous halide, MO – metal oxide, MS – metal sulfide)

Repassivation potential in environments containing Cl^- and H_2S

To extend the model to systems containing H_2S, we consider competitive adsorption of H_2S, Cl^- ions and water. The coverage fractions of H_2S, Cl^-, and H_2O on a surface corroding in the active state are denoted by θ_s, θ_c, and θ_o, respectively. The reactions at the metal surface may further lead to the formation of a metal oxide MO and metal sulfide MS. The surface coverage fractions of MO and MS are denoted by Ψ_{MO} and Ψ_{MS}, respectively. In systems that do not contain other electrochemically active species, the surface fractions satisfy the balance equation

$$\theta_c + \theta_s + \theta_o + \Psi_{MO} + \Psi_{MS} = 1 \tag{7}$$

Adsorption of Cl^- ions can be considered as a replacement of H_2O on the metal surface (M) with Cl^-, i.e.,

$$\underset{\theta_o}{MH_2O_{ads}} + Cl^- \underset{r_c^{\leftarrow}}{\overset{r_c^{\rightarrow}}{\rightleftharpoons}} \underset{\theta_c}{MCl^-_{ads}} + H_2O \tag{8}$$

where $r_c^{\rightarrow}$ and $r_c^{\leftarrow}$ are the adsorption and desorption rate constants, respectively. M is a metal whose properties are an appropriate average of those of the alloy components. In accordance with the previous studies,[5, 6] the adsorption is followed by the dissolution of the adsorbed complex, i.e.,

$$\underset{\theta_c}{MCl^-_{ads}} \xrightarrow{i_c} M^{z+} + ze^- + Cl^- \tag{9}$$

where i_c is the current density associated with the dissolution of the MCl^-_{ads} complex and z is the average charge. The process of repassivation is associated with the formation of a metal oxide layer according to the reaction:

$$\underset{\theta_o}{MH_2O_{ads}} + (z/2-1)H_2O \xrightarrow{i_{MO}} \underset{\Psi_{MO}}{MO_{z/2}} + zH^+ + ze^- \tag{10}$$

where i_o is the current density that is associated with the formation of the oxide. It is important to consider the presence of adsorbed H_2O in eqs. (8) and (10) because water is the necessary precursor for the formation of the oxide.[23] The surface oxide $MO_{z/2}$ can be further dissolved through a chemical dissolution process, i.e.,

$$\underset{\Psi_{MO}}{MO_{z/2}} + zH^+ \xrightarrow{k_{MO}} M^{z+} + (z/2)H_2O \tag{11}$$

where k_{MO} is a chemical dissolution rate constant. The effect of nitrogen on the repassivation of duplex alloys is not explicitly considered in this scheme and is incorporated into the empirical parameters of the model.

The presence of H_2S gives rise to electrochemical reactions that may lead to a very significant enhancement of the anodic dissolution process and may result in the formation of a sulfide phase. The mechanisms of the H_2S-induced acceleration of anodic dissolution were extensively studied in the literature for Fe,[7, 8, 10, 11, 13, 14] Ni,[8, 9, 12, 16] Cr,[15] and Fe-Ni-Cr-Mo alloys.[17, 18] In this study, we adopt a simplified version of a previously proposed mechanism.[7, 10, 13, 16] The mechanism needs to be simplified because, in view of the available data, it is not possible to separate the reactions of the individual alloy components and it is necessary to limit the number of parameters that can be numerically evaluated to characterize the mechanism. Thus, the adsorption of H_2S can be written as

$$\underset{\theta_o}{MH_2O_{ads}} + H_2S \underset{r_s^{\leftarrow}}{\overset{r_s^{\rightarrow}}{\rightleftharpoons}} \underset{\theta_s}{MHS^-_{ads}} + H^+ + H_2O \tag{12}$$

where $r_s^{\rightarrow}$ and $r_s^{\leftarrow}$ are the H_2S adsorption and desorption rate constants, respectively. The adsorption is followed by an electrochemical step:

$$MHS_{ads}^{-} \longrightarrow MHS_{ads}^{(z-1)+} + ze^{-} \tag{13}$$

Reaction (13) can be then followed by a dissolution reaction, which is responsible for the acceleration of the anodic process, i.e.,

$$MHS_{ads}^{(z-1)+} + H^{+} \longrightarrow M^{z+} + H_2S \tag{14}$$

or it can be followed by the formation of a solid metal sulfide phase:

$$MHS_{ads}^{(z-1)+} + (z/2-1)H_2S \longrightarrow MS_{z/2} + (z-1)H^{+} \tag{15}$$

In reaction (15), we can assume in practice that the effective formula of the metal sulfide is MS because NiS and mixed Ni-Fe sulfides are the predominant sulfides that may form on Fe-Ni-Cr alloys in aqueous solutions.[19, 22] By adding eqs. (13) and (14), we obtain

$$\underset{\theta_s}{MHS_{ads}^{-}} + H^{+} \xrightarrow{i_s} M^{z+} + H_2S + ze^{-} \tag{16}$$

where i_s is the current density associated with the H_2S-induced acceleration of anodic dissolution. Further, by adding eqs. (13) and (15), we obtain

$$\underset{\theta_s}{MHS_{ads}^{-}} + (z/2-1)H_2S \xrightarrow[\Psi_{MS}]{i_{MS}} MS_{z/2} + (z-1)H^{+} + ze^{-} \tag{17}$$

where i_{MS} is the current density for the formation of the metal sulfide. Thus, the mechanism reflects the competitive formation of metal oxide (eq. 10) and metal sulfide (eq. 17). This is illustrated schematically in Fig. 2 and is in agreement with the experiments of Marcus and Grimal,[20] who observed the formation of islands of chromium oxide and nickel sulfide on a surface. The sulfur islands were found to persist even in a passivated system.

The metal sulfide may undergo chemical dissolution according to the reactions

$$\underset{\Psi_{MS}}{MS_{z/2}} + zH^{+} \xrightarrow{k_{MS}} M^{z+} + (z/2)H_2S \tag{18}$$

$$\underset{\Psi_{MS}}{MS_{z/2}} + (2-z/2)H_2S \xrightarrow{u_{MS}'} M(HS)_2^{z-2} + (2-z)H^{+} \tag{19}$$

where the second reaction recognizes the possibility of formation of complex aqueous species such as $Fe(HS)_2^0$ or $Ni(HS)_2^0$, whose existence has been postulated in thermodynamic studies.[24]

After defining the reactions that may occur in the system in the process of repassivation, the change of coverage fractions with time can be related to the current densities and rate constants defined above. Based on eqs. (8) and (9), the change of the Cl^- coverage fraction is

$$\frac{\partial \theta_c}{\partial t} = r_c^{\rightarrow}\theta_o a_c(2) - r_c^{\leftarrow}\theta_c - c_c i_c \tag{20}$$

where $a_c(2)$ is the activity of Cl^- at the metal surface, c_c is a constant and the current density i_c is related to θ_c in accordance with reaction (9):

$$i_c = i_c^0 \theta_c \tag{21}$$

where the symbol i_c^0 is introduced to simplify further notation and is given by

$$i_c^0 = d_c \exp\left[\frac{\alpha_c F \Delta\Phi_{M/MX}(1,2)}{RT}\right] \quad (22)$$

From eqs. (10) and (11), the rate of formation of the oxide is given by

$$\frac{\partial \Psi_{MO}}{\partial t} = c_{MO} i_{MO} - k_{MO} \Psi_{MO} \quad (23)$$

where the current density i_{MO} is related to θ_o according to reaction (10):

$$i_{MO} = i_{MO}^0 \theta_0 \quad (24)$$

where

$$i_{MO}^0 = d_{MO} \exp\left[\frac{\xi_{MO} F \Delta\Phi_{M/MX}(1,2)}{RT}\right] \quad (25)$$

The change in the H_2S surface coverage fraction results analogously from reactions (12), (16), and (17):

$$\frac{\partial \theta_s}{\partial t} = r_s^{\rightarrow} \theta_o a_s(2) - r_s^{\leftarrow} \theta_s - c_{MS} i_{MS} - c_s i_s \quad (26)$$

where $a_s(2)$ is the activity of H_2S at the metal surface, c_{MS} and c_s are constants, i_{MS} is the current density that is responsible for the formation of the metal sulfide according to reaction (17):

$$i_{MS} = i_{MS}^0 \theta_s \quad (27)$$

where

$$i_{MS}^0 = d_{MS} \exp\left[\frac{\xi_{MS} F \Delta\Phi_{M/MX}(1,2)}{RT}\right] \quad (28)$$

and the current density that accounts for H_2S-accelerated dissolution is

$$i_s = i_s^0 \theta_s \quad (29)$$

where i_s^0 is given by

$$i_s^0 = d_s \exp\left[\frac{\alpha_s F \Delta\Phi_{M/MX}(1,2)}{RT}\right] \quad (30)$$

In eq. (28), we assume that $z = 2$ in reaction (17). The rate of formation of the sulfide layer is expressed as

$$\frac{\partial \Psi_{MS}}{\partial t} = c_{MS} i_{MS} - k_{MS} \Psi_{MS} - u_{MS}' a_s(2) \Psi_{MS} = c_{MS} i_{MS} - k_{MS} \Psi_{MS} \left(1 + u_{MS} a_s(2)\right) \quad (31)$$

where the first term on the right-hand side of eq. (31) is a consequence of reaction (17) and the second and third terms result from reactions (18) and (19), respectively.

The total anodic current density is a sum of those for the individual processes, i.e.,

$$i = i_c + i_{MO} + i_s + i_{MS} \quad (32)$$

In the steady state, which corresponds to the limit of repassivation, the surface coverage fractions no longer undergo a change. Hence,

$$\frac{\partial \theta_c}{\partial t} = \frac{\partial \Psi_{MO}}{\partial t} = \frac{\partial \theta_s}{\partial t} = \frac{\partial \Psi_{MS}}{\partial t} = 0 \tag{33}$$

The condition (33), together with eqs. (20), (23), (26), and (31), gives four equations that depend on θ_c, θ_o, Ψ_{MO}, θ_s, and Ψ_{MS}. By substituting θ_o from the surface coverage balance equation (7), the five variables θ_c, θ_o, Ψ_{MO}, θ_s, and Ψ_{MS} can be obtained analytically. Then, these variables are substituted into the defining equations for i_c, i_{MO}, i_{MS}, and i_s (eqs. 21-22, 24-25, 27-28, and 29-30, respectively) and the resulting expressions for current densities are summed according to eq. (32). The resulting expression for the total current density is:

$$i = \frac{\left[i_c^0 \frac{r_c^{\rightarrow} a_c(2)}{r_c^{\leftarrow}} + i_{MO}^0 \left(1 + \frac{c_c i_c^0}{r_c^{\leftarrow}} \right) \right] \left(1 + \frac{c_{MS} i_{MS}^0}{r_s^{\leftarrow}} + \frac{c_s i_s^0}{r_s^{\leftarrow}} \right) + \left(i_{MS}^0 + i_s^0 \right) \frac{r_s^{\rightarrow} a_s(2)}{r_s^{\leftarrow}} \left(1 + \frac{c_c i_c^0}{r_c^{\leftarrow}} \right)}{\left[1 + \frac{c_c i_c^0}{r_c^{\leftarrow}} + \frac{r_c^{\rightarrow} a_c(2)}{r_c^{\leftarrow}} + \frac{c_{MO} i_{MO}^0}{k_{MO}} \left(1 + \frac{c_c i_c^0}{r_c^{\leftarrow}} \right) \right] \left(1 + \frac{c_{MS} i_{MS}^0}{r_s^{\leftarrow}} + \frac{c_s i_s^0}{r_s^{\leftarrow}} \right) + \frac{r_s^{\rightarrow} a_s(2)}{r_s^{\leftarrow}} \left(1 + \frac{c_c i_c^0}{r_c^{\leftarrow}} \right) \left(1 + \frac{c_{MS} i_{MS}^0}{k_{MS}(1 + u_{MS}'' a_s(2))} \right)} \tag{34}$$

Eq. (34) can be solved in the limit of repassivation, i.e., when $E = E_{rp}$ and $i = i_{rp}$. For this purpose, we utilize eqs. (5) and (6), which are valid in the repassivation limit. Then, eq. (34) becomes

$$i_{rp} = \frac{\left[i_c^0 r_c a_c + i_{MO}^0 \left(1 + e_c i_c^0 \right) \right] \left(1 + e_{MS} i_{MS}^0 + e_s i_s^0 \right) + \left(i_{MS}^0 + i_s^0 \right) r_s a_s \left(1 + e_c i_c^0 \right)}{\left[1 + e_c i_c^0 + r_c a_c + \frac{i_{MO}^0}{i_p} \left(1 + e_c i_c^0 \right) \right] \left(1 + e_{MS} i_{MS}^0 + e_s i_s^0 \right) + r_s a_s \left(1 + e_c i_c^0 \right) \left(1 + \frac{i_{MS}^0}{i_q (1 + u_{MS} a_s)} \right)} \tag{35}$$

where $r_c = r_c^{\rightarrow} / (r_c^{\leftarrow} K_3)$ and $r_s = r_s^{\rightarrow} / (r_s^{\leftarrow} K_3)$ are rescaled adsorption equilibrium constants for Cl^- and H_2S, respectively, $e_c = c_c / r_c^{\leftarrow}$, $e_s = c_s / r_s^{\leftarrow}$, $e_{MS} = c_{MS} / r_c^{\leftarrow}$, $i_p = k_{MO} / c_{MO}$, $i_q = k_{MS} / c_{MS}$ and $a_c = a_c(5)$ and $a_s = a_s(5)$ are the activities of Cl^- and H_2S, respectively, in the bulk environment. In the limit of repassivation, the expressions for i_c^0, i_{MO}^0, i_{MS}^0, and i_s^0 take the form:

$$i_c^0 = d_c \exp\left[\frac{\alpha_c F (E_{rp} - K_1)}{RT} \right] = f_c \exp\left[\frac{\alpha_c F E_{rp}}{RT} \right] \tag{36}$$

$$i_{MO}^0 = d_{MO} \exp\left[\frac{\xi_{MO} F (E_{rp} - K_1)}{RT} \right] = f_{MO} \exp\left[\frac{\xi_{MO} F E_{rp}}{RT} \right] \tag{37}$$

$$i_{MS}^0 = d_{MS} \exp\left[\frac{\xi_{MS} F (E_{rp} - K_1)}{RT} \right] = f_{MS} \exp\left[\frac{\xi_{MS} F E_{rp}}{RT} \right] \tag{38}$$

$$i_s^0 = d_s \exp\left[\frac{\alpha_s F (E_{rp} - K_1)}{RT} \right] = f_s \exp\left[\frac{\alpha_s F E_{rp}}{RT} \right] \tag{39}$$

Eq. (35), coupled with eqs. (36-39), constitutes the fundamental equation for finding the value of E_{rp}. However, it needs to be simplified for a practical application of the model.

Practical implementation of the model

To make the model manageable with respect to the number of parameters, we observe that the coefficients e_c, e_s, and e_{MS} can be neglected. This is due to the fact that, at the low current densities at repassivation, the desorption terms in eqs. (20) and (26) that are due to the current densities are less significant than the physical desorption terms. Also, preliminary numerical tests have revealed that the terms that contain the e_c, e_s, and e_{MS} coefficients can be neglected. Then, eq. (35) reduces to:

$$i_{rp} = \frac{i_c^0 r_c a_c + i_{MO}^0 + \left(i_{MS}^0 + i_s^0\right) r_s a_s}{1 + r_c a_c + \frac{i_{MO}^0}{i_p} + r_s a_s \left(1 + \frac{i_{MS}^0}{i_q \left(1 + u_{MS} a_s\right)}\right)} \quad (40)$$

The repassivation potential is then obtained numerically by solving a single nonlinear equation with respect to E_{rp}, i.e., eq. 40 with i_c, i_{MO}, i_{MS}, and i_s defined by eqs. (36-39). The activities a_c and a_s are calculated from an electrolyte thermodynamic model.[5]

As in the previous study,[5] it is convenient to express the rate constants f_j (j = c, MO, MS, or s) in eqs. (36-39) using corresponding Gibbs energies of activation, i.e.,

$$f_j = \exp\left(-\frac{\Delta g_j^{\neq}}{RT}\right) \quad (41)$$

where j = c, MO, s, or MS. An analogous equation expresses the dissolution rate constant u_{MS} in terms of a corresponding Gibbs energy of activation, $\Delta g_{dis,MS}^{\neq}$. The Gibbs energy of activation may be temperature-dependent according to the relation:

$$\frac{\Delta g_j^{\neq}}{RT} = \frac{\Delta g_j^{\neq}(T_{ref})}{RT_{ref}} + \Delta h_j^{\neq}\left(\frac{1}{T} - \frac{1}{T_{ref}}\right) \quad (42)$$

where T_{ref} is a reference temperature (T_{ref} = 298.15K). The adsorption equilibrium constants are expressed using a Gibbs energy of adsorption, i.e.,

$$r_j = \exp\left(-\frac{\Delta g_{ads,j}}{RT}\right) \quad (43)$$

where j = c and s. For the coefficient f_s in eq. (39), a first-order dependence on the activity of chlorides is assumed, i.e.,

$$f_s = f_s' a_c \quad (44)$$

where f_s' is expressed by eqs. (41-42). This reflects the synergistic effect of H_2S and Cl^- on anodic dissolution. The remaining coefficients f_j (j = c, MO, and MS) depend only on temperature according to eqs. (41-42). For simplicity, the electrochemical transfer coefficients α_c and α_s in eqs. 36 and 39 are assumed to be 1. The constants i_p and i_q in eq. (40) are assigned the value 10^{-4} A/m^2. This is due to the fact that i_p is equal to the passive current density,[5] for which 10^{-4} A/m^2 is a reasonable approximation for CRAs. The constant i_q can be expected to have a comparable value.

RESULTS

First, the model has been applied to alloy S41425 in chloride-only environments because such environments provide a baseline for analyzing the effect of H_2S. In addition to the new E_{rp} data reported in Table 3, a substantial number of experimental measurements is available from a previous study[6] for S41425 in Cl solutions at 23°C, 60°C, and 95°C. In Cl systems, the model is completely defined when six parameters are specified: the Gibbs energy $\Delta g_c^{\neq}(T_{ref})$ and enthalpy $\Delta h_c^{\neq}$ of activation for the anodic dissolution mediated by the adsorption of Cl^- ions (eqs. 36 and 41-42), the Gibbs energy $\Delta g_{MO}^{\neq}(T_{ref})$ and enthalpy $\Delta h_{MO}^{\neq}$ of activation for the formation of oxide (eqs. 37 and 41-42), the electrochemical transfer coefficient for the formation of oxide ξ_{MO} (eq. 37) and the Gibbs energy of adsorption of Cl^- ions $\Delta g_{ads,c}$ (eq. 43). Of these parameters, $\Delta h_{MO}^{\neq}$, ξ_{MO}, and $\Delta g_{ads,c}$ are obtained from a previously

developed generalized correlation[6] and only the three remaining parameters (i.e., $\Delta g_c^{\neq}(T_{ref})$, $\Delta h_c^{\neq}$, and $\Delta g_{MO}^{\neq}(T_{ref})$) have been adjusted to match the data. These parameters are listed in Table 3. With these parameters, the model can accurately reproduce the experimental E_{rp} data as a function of chloride concentration and temperature. This is illustrated in Fig. 3, which compares the calculated results with the data. As shown in Fig. 3, the E_{rp} vs. chloride activity plot shows a typical pattern of a lower slope at higher Cl concentrations and a higher slope at lower concentrations. Significant temperature dependence is observed only at lower concentrations whereas the E_{rp} curves for various temperatures almost coincide at higher Cl concentrations.

Table 3. Parameters of the repassivation potential model and their values for Cl^- H_2S systems. The Gibbs energy and enthalpy values are given in kJ/mol.

Model parameter	Parameter definition	Alloy	
		S41425	S32750
$\Delta g_c^{\neq}(T_{ref})$	Gibbs energy of activation for dissolution mediated by adsorption of Cl^- at reference T	-9.6	20.0
$\Delta h_c^{\neq}$	Enthalpy of activation for dissolution mediated by Cl^- adsorption	-44	24
$\Delta g_{ads,c}$	Gibbs energy of adsorption of Cl^-	10	10
$\Delta g_{MO}^{\neq}(T_{ref})$	Gibbs energy of activation for oxide formation at reference temperature	27.0	20.6
$\Delta h_{MO}^{\neq}$	Enthalpy of activation for oxide formation	-49	-83
ξ_{MO}	Electrochemical transfer coefficient for oxide formation	0.8	0.8
$\Delta g_s^{\neq}(T_{ref})$	Gibbs energy of activation for dissolution mediated by adsorption of H_2S at reference T	-14.5	assumed the same as for S41425
$\Delta g_{ads,s}$	Gibbs energy of adsorption of H_2S	-23.0	
$\Delta g_{MS}^{\neq}(T_{ref})$	Gibbs energy of activation for sulfide formation at reference T	3.8	
ξ_{MS}	Electrochemical transfer coefficient for sulfide formation	0.7	
$\Delta g_{dis,MS}^{\neq}$	Gibbs energy of activation for sulfide dissolution	-21.7	

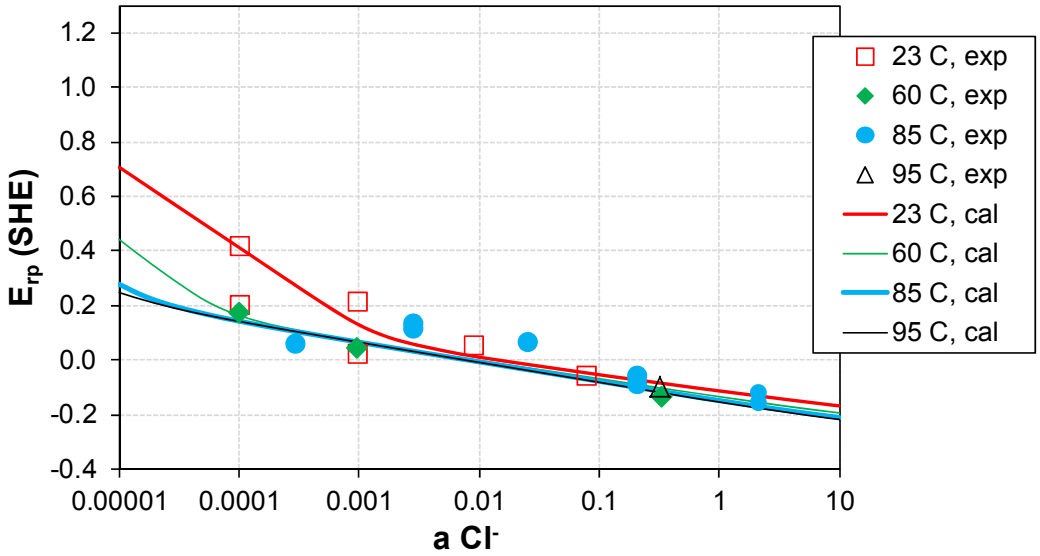

Figure 3. Repassivation potential of alloy S41425 in chloride solutions as a function of Cl^- activity at various temperatures. The symbols are the measurements from a previous study[6] and Table 3 and the lines have been obtained from the model.

After establishing the model for chloride-only systems, parameters have been determined for Cl – H_2S systems. These parameters include the Gibbs energy of adsorption of H_2S ($\Delta g_{ads,s}$), the Gibbs energies of activation for H_2S-accelerated dissolution, metal sulfide formation, and sulfide chemical dissolution ($\Delta g_s^{\neq}(T_{ref})$, $\Delta g_{MS}^{\neq}(T_{ref})$, and $\Delta g_{dis,MS}^{\neq}$, respectively), and the electrochemical transfer coefficient for sulfide formation (ξ_{MS}). The corresponding enthalpies of activation are assumed to be zero. These parameters are included in Table 3 and the results of calculations are shown in Fig. 4. Fig. 4 indicates that the effect of H_2S on the repassivation potential is very complex. At high H_2S concentrations (100 wt%), the E_{rp} vs. Cl^- curve is almost parallel to that in the absence of H_2S but it is shifted towards lower potentials by about 0.2 V. This is a manifestation of the acceleration of anodic dissolution in the localized environment by the presence of H_2S. As a result, H_2S strongly increases the tendency of the alloy to undergo localized corrosion at all Cl concentrations. On the other hand, the effect of H_2S at lower H_2S concentrations (i.e., 1 wt%) strongly depends on the chloride concentration. At high chloride concentrations, there is little difference between the behavior of systems with 1% and 100% H_2S. This is due to the fact that the adsorption of H_2S is very strong and, therefore, there is not much difference between the availability of adsorbed sulfur on the surface at the two vapor-phase compositions. However, a drastically different behavior is observed at low chloride concentration. In the low-Cl range, there is no reduction in E_{rp} due to H_2S and, instead, E_{rp} increases even above its level in Cl-only solutions. This effect is due to the formation of solid metal sulfide in competition with metal oxide. The presence of metal sulfide has a strong inhibitive effect. The net behavior of the system is a result of the competition between the acceleration of anodic dissolution due to the adsorption of H_2S and the inhibition due to the formation of a solid sulfide phase. The model correctly represents the complex dependence of E_{rp} on Cl^- and H_2S concentration, which results from this competition.

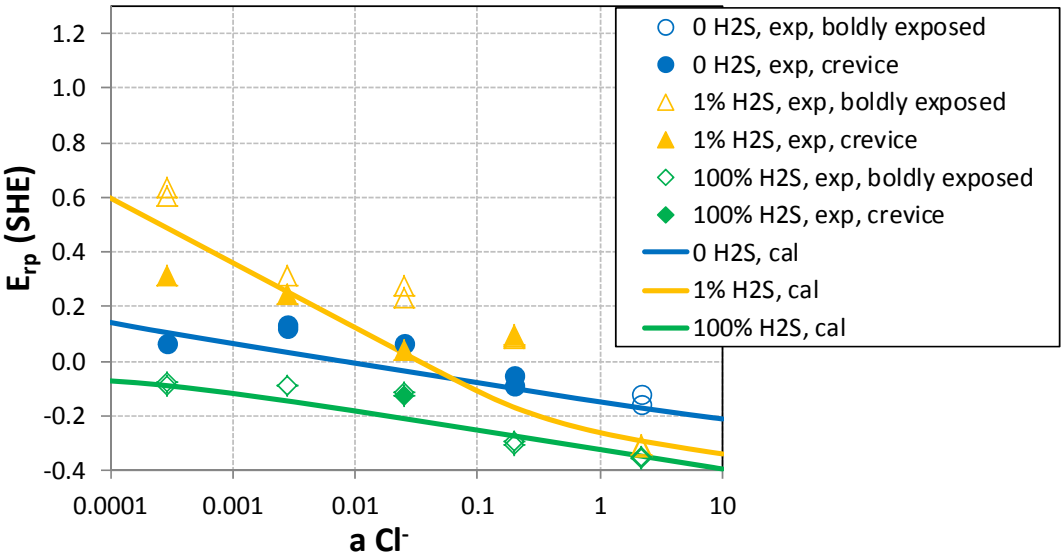

Figure 4. Repassivation potential of S41425 at 85°C in Cl^- + H_2S systems as a function of Cl^- activity at three concentrations of H_2S in the gas phase (0, 1, and 100 wt%). The lines have been obtained from the model.

To verify the model further, it is necessary to analyze the behavior of more corrosion-resistant alloys such as the duplex alloy S32750. The results for this alloy are shown in Fig. 5. In this case, the E_{rp} values in Cl-only environments are much higher than for S41425. This is due to the much higher Cr, Mo, and N content of alloy S32750. Substantial scattering of experimental data is observed at low Cl concentrations because of the high values of E_{rp}, which reflect the inherent difficulty in obtaining stable localized corrosion. It is remarkable that the presence of H_2S results in a very large decrease in E_{rp} (by

more than 0.4 V). Thus, the relative effect of H_2S is much stronger for alloy S32750 at high Cl concentrations than for the less corrosion-resistant alloy S41425. To model the effect of H_2S, the necessary parameters have been assumed to be the same as for S41425. As shown in Fig. 5, the prediction for a 100% H_2S environment is very close to the experimental data point. Thus, the increased susceptibility to localized corrosion is correctly predicted. For a further verification of the model, more data will be necessary for alloy S32750 at lower Cl and H_2S concentration. Also, further studies will be focused on other martensitic stainless steels and Ni-base alloys.

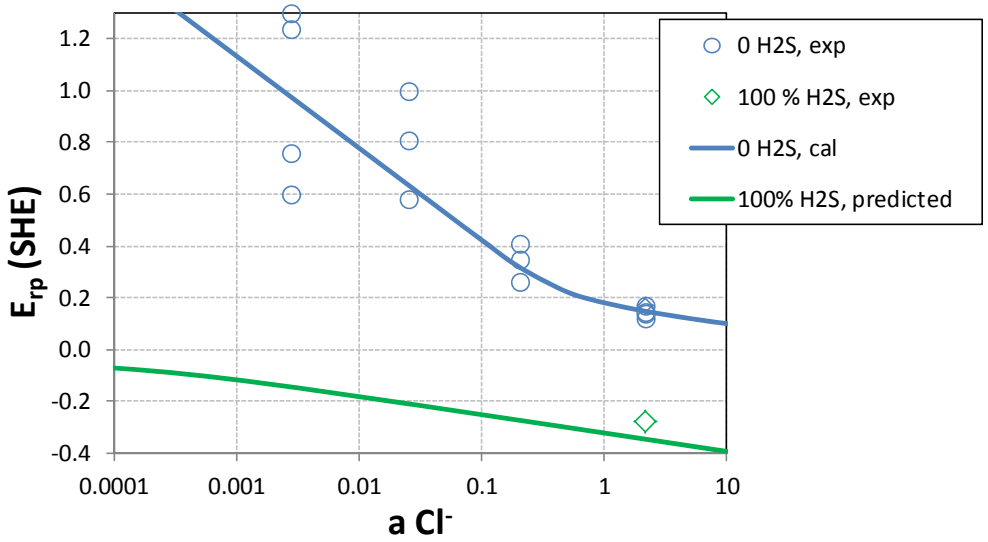

Figure 5. Calculated and experimental repassivation potentials of alloy S32750 at 85°C.

CONCLUSIONS

- A systematic study has been undertaken to provide the values of the repassivation potential of corrosion-resistant alloys as a criterion for predicting whether the alloys can undergo localized corrosion and stress corrosion cracking in oil and gas-related environments.
- A comprehensive set of E_{rp} data has been obtained for the S41425 stainless steel in Cl^- + H_2S environments and more limited data have been measured for alloy S32750.
- A model for calculating the repassivation potential as a function of solution chemistry and temperature has been developed. The model considers competitive adsorption, enhancement of anodic dissolution due to the adsorption of electrochemically active species and competitive formation of metal oxide and sulfide in the process of repassivation.
- The presence of H_2S can substantially reduce the repassivation potential, thus indicating a strongly enhanced tendency for localized corrosion and stress corrosion cracking. However, exceptions exist at lower H_2S and Cl^- concentrations. This complex behavior is accurately represented by the model. Furthermore, the model can be used for predicting the repassivation potential of alloys for which E_{rp} data have not been previously determined.

ACKNOWLEDGEMENT

The work reported here was supported by Chevron, ConocoPhillips, DNV, JFE, Petrobras, Sandvik, Sumitomo Metals, and Vallourec-Manesmann within the framework of the joint industry program “Performance Assessment of CRAs in Severe Well Environments.”

REFERENCES

1. NACE: 'Laboratory Testing of Metals for Resistance to Sulfide Stress Cracking and Stress Corrosion Cracking in H_2S Environments', *NACE Standard TM0177-2005*, 2005.

2. NACE/ISO: 'Petroleum and Natural Gas Industries - Materials for Use in H_2S-Containing Environments in Oil and Gas Production ', *NACE MR0175/ISO 15156-2 Int. Standard*, 2009.
3. P. R. Rhodes: 'Environment-Assisted Cracking of Corrosion-Resistant Alloys in Oil and Gas Production Environments: A Review', *Corrosion*, 2001, **57**(11), 923-966.
4. G. A. Cragnolino, D. S. Dunn, Y.-M. Pan, and N. Sridhar: 'The Critical Potential for the Stress Corrosion Cracking of Fe-Ni-Cr Alloys and its Mechanistic Implications', *Chemistry and Electrochemicatry of Corrosion and Stress Corrosion Cracking: A Symposium Honoring the Contributions of R.W. Staehle. TMS Annual Meeting, New Orleans*, 2001, 83-104.
5. A. Anderko, N. Sridhar, and D. S. Dunn: 'A General Model for the Repassivation Potential as a Function of Multiple Aqueous Solution Species', *Corrosion Science*, 2004, **46**(7), 1583-1612.
6. A. Anderko, N. Sridhar, M. A. Jakab, and G. Tormoen: 'A General Model for the Repassivation Potential as a Function of Multiple Aqueous Species. 2. Effect of Oxyanions on Localized Corrosion of Fe-Ni-Cr-Mo-W-N Alloys', *Corrosion Science*, 2008, **50**(12), 3629-3647.
7. Z. A. Iofa, V. V. Batrakov, and Cho-Ngok-Ba: 'Influence of Anion Adsorption on the Action of Inhibitors on the Acid Corrosion of Iron and Cobalt', *Electrochim. Acta*, 1964, **9**, 1645-1653.
8. P. Süry: 'Similarities in the Corrosion Behavior of Iron, Cobalt and Nickel in Acid Solutions. A Review with Special Reference to the Sulphide Adsorption', *Corrosion Science*, 1976, **16**, 879-901.
9. J. Oudar and P. Marcus: 'Role of Adsorbed Sulphur in the Dissolution and Passivation of Nickel and Nickel-Sulphur Alloys', *Applications of Surface Science*, 1979, **3**, 48-67.
10. D. W. Shoesmith, P. Taylor, M. G. Bailey, and D. G. Owen: 'The Formation of Ferrous Monosulfide Polymorphs during the Corrosion of Iron by Aqueous Hydrogen Sulfide at 21°C', *J. Electrochem. Soc.*, 1980, **127**(5), 1007-1015.
11. D. R. Morris, L. P. Sampaleanu, and D. N. Veysey: 'The Corrosion of Steel by Aqueous Solutions of Hydrogen Sulfide', *J. Electrochem. Soc.*, 1980, **127**(6), 1228-1235.
12. S. Ando, T. Suzuki, and K. Itaya: 'Layer-by-Layer Anodic Dissolution of Sulfur-Modified Ni(100) Electrodes: In Situ Scanning Tunneling Microscopy', *J. Electroanal. Chem.*, 1996, **412**, 139-146.
13. H. Y. Ma, X. L. Cheng, S. H. Chen, C. Wang, J. P. Zhang, and H. Q. Yang: 'An AC Impdedance Study of the Anodic Dissolution of Iron in Sulfuric Acid Solutions Containing Hydrogen Sulfide', *J. Electroanalytical Chem.*, 1998, **451**, 11-17.
14. X. L. Cheng, H. Y. Ma, J. P. Zhang, X. Chen, S. H. Chen, and H. Q. Yang: 'Corrosion of Iron in Acid Solutions with Hydrogen Sulfide', *Corrosion*, 1998, **54**(5), 369-376.
15. X. L. Cheng, H. Y. Ma, S. H. Chen, L. Niu, S. B. Lei, R. Yu, and Z. M. Yao: 'Electrochemical Behavior of Chromium in Acid Solutions with H_2S', *Corrosion Science*, 1999, **41**, 773-788.
16. X. L. Cheng, H. Y. Ma, S. H. Chen, X. Chen, and Z. M. Yao: 'Corrosion of Nickel in Acid Solutions with Hydrogen Sulfide', *Corrosion Science*, 2000, **42**, 299-311.
17. A. Elbiache and P. Marcus: 'The Role of Molybdenum in the Dissolution and the Passivation of Stainless Steel with Adsorbed Sulphur', *Corrosion Science*, 1992, **33**(2), 261-269.
18. A. J. Betts and R. C. Newman: 'The Effect of Alloyed Molybdenum on the Activation of Anodic Dissolutions by Reduced Sulphur Compounds', *Corrosion Science*, 1993, **34**(9), 1551-1555.
19. P. Marcus, I. Olefjord, and J. Oudar: 'The Influence of Sulphur on the Dissolution and the Passivation of a Nickel-Iron Alloy - II. Surface Analysis by ESCA', *Corrosion Science*, 1984, **24**(4), 269-278.
20. P. Marcus and J. M. Grimal: 'The Antagonistic Roles of Chromium and Sulphur in the Passivation of Ni-Cr-Fe Alloys Studied by XPS and Radiochemical Techniques', *Corrosion Science*, 1990, **31**, 377-382.
21. S. Azuma, H. Tsuge, T. Kudo, and T. Moroishi: 'Crevice Corrosion of Duplex Stainless Steel in Simulated Sour Gas Environments', *Corrosion*, 1989, **45**(3), 235-242.
22. S. Azuma and T. Kudo: 'Crevice Corrosion of Corrosion-Resistant Alloys in Simulated Sour Gas Environments', *Corrosion*, 1991, **47**(6), 458-463.
23. T. Okada: 'Considerations of the Stability of Pit Repassivation during Pitting Corrosion of Passive Metals', *J. Electrochem. Soc.*, 1984, **131**, 1026-1032.
24. D. Rickard: 'The Solubility of FeS', *Geochim. Cosmochim. Acta*, 2006, **70**, 5779-5789.